# X-ray Reflectivity Study of a Monolayer of Ferritin Proteins at a Nanofilm Aqueous−Aqueous Interface

**Ming Li,[†,‡] David J. Chaiko,[§] and Mark L. Schlossman*[,‡,||]**

*Department of Physics, University of Illinois at Chicago, 845 West Taylor Street, Chicago, Illinois 60607, Argonne National Laboratory, 9700 South Cass Avenue, Argonne, Illinois 60439, and Department of Chemistry, University of Illinois at Chicago, 845 West Taylor Street, Chicago, Illinois 60607*

*Received: February 7, 2003; In Final Form: June 9, 2003*

The formation of thin aqueous films on top of an aqueous subphase is demonstrated. The films form through a complex spreading process that results in the coexistence of macroscopic lenses and films that are several nanometers thick. Aqueous biphase solutions of poly(ethylene glycol), potassium phosphates, and water are used to form these films. Synchrotron X-ray scattering is used to characterize the structure of the thin film and to probe the adsorption of proteins to the film. X-ray reflectivity measures the layer thickness (4−5 nm) and the roughness of the two interfaces of the film. Surface and interfacial tension measurements, combined with the X-ray measurements, indicate that the films are a thin layer of the bulk solution rather than a monolayer of PEG molecules. The film can be described by an excess free energy with a short range piece (due primarily to capillary wave entropic repulsion) and a long-range van der Waals interaction. Biomolecules, such as proteins, can be trapped at the aqueous−aqueous interface or in the thin film. This idea is demonstrated by an X-ray reflectivity study of ferritin proteins that form a 2-dimensional array at the interface. It is shown that the electron density interfacial profile of the ferritin trapped in this thin film is consistent with the known crystal structure of ferritin. In the absence of the thin film, ferritin does not adsorb to the interface.

## Introduction

Aqueous mixtures of polymers, salts, and water are known to phase separate into two or more equilibrium phases.[1,2] The simplest mixtures consist of either a single polymer species and a salt (and water) or two different polymer species (and water) and form biphase mixtures under appropriate conditions. Aqueous biphase systems are used, for example, for the purification and separation of biological materials.[1,2] The components can be chosen to provide an appropriate environment for biological macromolecules, such as proteins, that allow them to be purified without denaturing. Poly(ethylene glycol) (PEG) is often used as one component. PEG is used in many aspects of handling proteins, for example, to improve the biocompatibility of artificial materials used in clinical practice, to reduce the immune response of proteins attached to PEG, and to aid 3-dimensional crystallization, among others.[3−7]

Liquid surfaces have been used to assemble protein arrays or to crystallize proteins that are difficult to crystallize in 3-dimensions. As examples, Nagayama and co-workers spread 2-d protein arrays from aqueous spreading solutions onto a mercury surface.[8,9] Nagayama et al. also demonstrated the formation of protein arrays at the air−water (glucose solution) interface by injecting a drop of a protein solution into the bulk of the glucose solution. The drop rises to the surface and it is believed that some of the proteins unfold at the water−air interface whereas others form a 2-d crystal immediately below the denatured protein film.[8,10] These arrays were then transferred to electron microscopy grids for study by electron diffraction. Fujiyoshi and co-workers studied the formation of 2-dimensional protein crystals at the water−oil interface, also extracting them for analysis by electron microscopy.[11] An extensive effort has been devoted to the production of 2-dimensional protein crystals by a variety of methods, including their growth on lipid monolayers at the air−water interface.[12−15] These have been particularly useful for structure determination by electron diffraction of membrane proteins, which are difficult to crystallize in three dimensions (for recent reviews, see Hasler et al. and Hebert).[16,17]

In this paper, we demonstrate the use of aqueous biphase solutions to form thin aqueous films on top of an aqueous subphase. The films are several nanometers thick and are formed from aqueous solutions of poly(ethylene glycol), potassium phosphates, and water. Because the film is very thin, X-rays penetrate through it with little absorption and X-ray scattering can be used to probe structure at the aqueous−aqueous interface. An earlier report of some of this work emphasized the use of X-ray off-specular diffuse scattering to probe the excess free energy of formation of this thin film.[18,19] Here, we show that a drop of protein solution (with ferritin proteins) added to the subphase will rise to the aqueous−aqueous interface and spread the proteins at the interface. The molecular ordering normal to the interface is probed by X-ray reflectivity. The measured electron density profile is consistent with the crystallographic structure of ferritin, indicating that the ferritin is not denatured at the interface. This is likely due to the presence of the thin PEG-rich film. A control experiment performed without the PEG-rich film did not yield a stable layer of ferritin. The concentration of ferritin at the interface is not large enough to form an ordered array that could be further studied with X-ray diffraction. However, it is reasonable to expect that future

* Corresponding author. E-mail: schloss@uic.edu.
[†] Current address: Ming Li, Institute of Physics, Chinese Academy of Sciences, Beijing 100080, P. R. China.
[‡] Department of Physics, University of Illinois at Chicago.
[§] Argonne National Laboratory.
[||] Department of Chemistry, University of Illinois at Chicago.

10.1021/jp0343281 CCC: $25.00 
Published on Web 07/17/2003

**TABLE 1: Solution Parameters**

| sample | temp (±0.03) (°C) | concentrations (% W/W)[a] overall (±0.1) PEG | overall (±0.1) salt | PEG* (±0.5) PEG | PEG* (±0.5) salt | salt* (±0.5) PEG | salt* (±0.5) salt | pH | tension γ (mN/m)[b] PEG* (±0.5) | salt* (±0.5) | salt*/PEG* |
|---|---|---|---|---|---|---|---|---|---|---|---|
| PEG3400 + $K_2HPO_4$ | 35 | 15.2 | 26.5 | 65.8 | 2.0 | 0.5 | 34.4 | 9.2[c] | 51.6 | 77.2 | 7 ± 1 |
| PEG8000 + $K_2HPO_4$:$KH_2PO_4$ (3:2) | 27.5 | 5.0 | 15.0 | 35.0 | 2.7 | 1.6 | 16.3 | ~7[c] | 60.1 | 63.0 | 0.5 ± 0.5 |

[a] Weight percentage concentrations. PEG* and salt* refer to the PEG-rich and salt-rich phases of the original biphase solution. We measure the overall concentrations; the concentrations of the individual phases are determined by phase diagrams in the literature.[2] The available phase diagram for the PEG8000 system is for a 2:1 ratio of $K_2HPO_4$:$KH_2PO_4$, which we quote as a reasonable guide for our 3:2 system. [b] PEG* tension is the surface tension measured at the PEG*−vapor interface; salt* tension is the surface tension measured at the salt*−vapor interface; salt*/PEG* tension is the interfacial tension measured at the salt*−PEG* interface. Interfacial and surface tensions were measured with the drop-weight[20] and Wilhelmy plate[21] methods, respectively. [c] pH values determined from the literature.

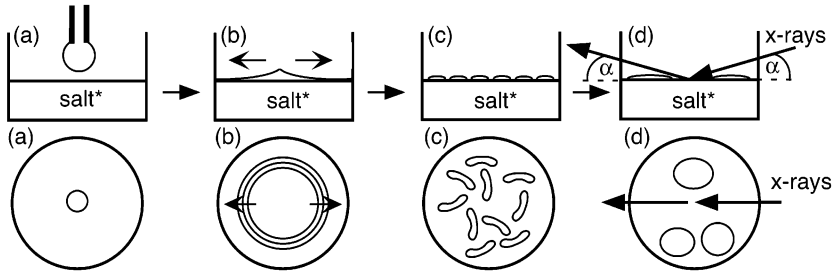


**Figure 1.** (a) Thin layer is formed by placing a drop of the PEG* phase on the surface of the salt-rich phase with a pipet (top cartoons are a side view, bottom are a top view). (b) Over a period of ~1 s the drop spreads and a ring of interference colors can be observed. (c) After about 10 s, small islands form that appear like a spinodal pattern (not as ordered as the cartoon). (d) The pattern coarsens over a period of ~1 h, leaving a few large (~1 cm diameter) lenses. The lenses are pushed aside with a pipet to allow access for the X-rays that probe the region between the lenses. Kinematics for specular reflectivity are shown in (d).

developments in sample preparation (such as adding more protein solution so there is enough ferritin to entirely cover the interface, or adjusting the concentration of the bulk aqueous solutions) would lead to 2-dimensional crystals at the aqueous−aqueous interface that could be studied with X-ray diffraction.

## Experimental Methods

**Materials and Tension Measurements.** We studied biphase mixtures of poly(ethylene glycol) (denoted as PEG; $H(OCH_2CH_2)_mOH$, $M_n = 3400$ or 8000, from Aldrich, used as received), potassium phosphates ($K_2HPO_4$ and $KH_2PO_4$ from Fluka, 99.5%, used as received), and Barnstead Nanopure water. The mixtures of water, salts, and PEG were shaken, allowed to equilibrate for at least 20 h at room temperature in a separatory funnel until the phases were clear. When the phases were extracted from the funnel, the region near the interface was discarded. The lighter top PEG-rich phase is denoted PEG* and the heavier salt-rich phase is denoted salt*. Table 1 lists the concentrations of the samples, the concentrations of individual phases, and the pH. The two different sample solutions will be referred to as PEG3400 or PEG8000. Experiments were performed with two different molecular weights of PEG to determine if the film thickness depended upon molecular weight. The interfacial and surface tensions were measured by the drop-weight and Wilhelmy plate methods and are also listed in Table 1.[20,21]

The experiments with ferritin used ferritin from horse spleen (Sigma,102 mg/mL ferritin in 0.15 M NaCl solution, iron content is 18 mg/mL) that we diluted by a 10% (W/W) PEG8000 solution (ferritin solution to PEG8000 solution ratio of 1:3). One microliter of this solution was added to the lower salt* phase (~40 mL) when ferritin adsorption in the presence of the thin PEG* film was studied (for the PEG8000 system); 6 μL was added when ferritin adsorption in the absence of the thin PEG* film was studied. This corresponds to a ferritin concentration in the lower phase of 0.7 or 4 nM, respectively. A similar range of concentrations were used to test for ferritin adsorption in the PEG3400 system. The protein solution was stored in a refrigerator no longer than 2 days prior to the X-ray measurements.

**Formation of Thin Films.** A vapor-tight Teflon sample cell contained a circular trough (60 mm diameter) for the liquid sample. A separate reservoir for pure water maintained a high humidity in the sample cell. The cell was contained in an aluminum thermostat that provided temperature control to ±0.03 °C. The temperatures for each sample are listed in Table 1 and were chosen to be in the two-phase region for the selected compositions. In this paper we show two representative sets of measurements for PEG3400 and PEG8000 samples. However, many samples were studied and we have found that these results are not sensitive to small changes in temperature (±5 °C).

A sample is prepared by first aspirating the surface of the bulk salt* phase, then a small drop of the PEG* phase is placed onto the surface of the salt* phase. The drop spreads across the entire surface and thins rapidly, as is evident from the rapidly changing optical interference pattern that spreads across the surface (see Figure 1). After a few seconds the thin layer becomes unstable and forms an irregular pattern. This pattern then coalesces over a period of about 1 h to form lenses of diameter on the order of 1 cm. Lenses in the path of the X-ray beam are either aspirated off the surface or moved off to the side (at least one lens remains on the surface during the X-ray measurements). The macroscopic lenses function as reservoirs for the thin film PEG* top phase. The results in this paper are independent of the precise volume of the initial drop, which can vary from fractions of a microliter to a couple of microliters (essentially the variation in size of small to large drops formed at the end of a syringe needle).

Several aspects of our measurements ensured that the X-rays probe the region of the surface without lenses. Visual observa-

tion of the sample before and after the X-ray measurement indicated that lenses were not in the path of the X-rays. Also, if lenses floated into the X-ray beam during a measurement, they would produce two effects that are immediately noticeable. First, they produce additional diffuse scattering that would be recorded by our measurements of the background taken throughout the reflectivity measurements. Second, they alter the X-ray alignment scans that traverse the entire sample surface along the direction of the beam. These latter scans are used throughout the reflectivity measurement to verify the sample alignment. Neither of these effects occurred for the data presented in this paper, indicating that the area probed by the X-rays did not contain lenses.

Because we believe that the thin PEG* film is in equilibrium with the PEG* lenses and the bulk salt* phase, it is reasonable to expect that spontaneous formation of the equilibrium thin film from the lower phase should occur. However, the salt* phase contains a vary small amount of PEG (see Table 1) and spontaneous formation of a PEG* thin film from the salt* phase is kinetically hindered. Our recent measurements confirm the existence of a spontaneously formed film after a sufficiently long period of waiting (and will be reported elsewhere). In this paper, the thin PEG* film was always formed by adding a drop as described above.

The ferritin samples are prepared by inserting a syringe needle through the thin PEG* layer and depositing a drop (or drops) of the ferritin solution into the bulk salt* phase. When several drops are used, they are added to different places in the sample.

**X-ray Methods.** X-ray reflectivity was conducted at beamline X19C at the National Synchrotron Light Source (Brookhaven National Laboratory) with a liquid surface spectrometer and measurement techniques described in detail elsewhere.[22,23] The kinematics of reflectivity is illustrated in Figure 1d; note that $\alpha = 90°$ is normal to the surface. For specular reflection, the wave vector transfer, $\mathbf{Q} = k_{\text{reflected}} - k_{\text{incident}}$, is only in the *z*-direction, normal to the interface; $Q_x = Q_y = 0$ where *x* and *y* are in the plane of the interface, and $Q_z = (4\pi/\lambda)\sin(\alpha)$. Therefore, specular reflection probes structure normal to the interface. Specifically, specular reflectivity probes the electron density normal to the interface and averaged over the region of the X-ray footprint on the sample. The X-ray wavelength $\lambda = 0.825 \pm 0.0004$ Å for studies of the PEG3400 samples and $\lambda = 1.540 \pm 0.0008$ Å for studies of the PEG8000 samples (it is preferable to use the longer wavelength to minimize scattering from the bulk liquid, however, considerations of efficient use of beamtime dictated our use of the smaller wavelength for the PEG3400 samples). The reflectivity data consist of measurements of the X-ray intensity reflected from the sample normalized to the incident intensity measured just before the X-rays strike the surface. These data are further modified by subtracting a background measured slightly off the specular condition by averaging intensity values at wave vector transfer $\mathbf{Q} = (0, \Delta Q_y, Q_z)$ and $\mathbf{Q} = (0, -\Delta Q_y, Q_z)$.[22] An incident slit (gap $\geq 20$ $\mu$m) determines the beam size on the sample and a slit (gap $\geq 200$ $\mu$m) before the detector sets the resolution of the measurement. The footprint of the beam on the sample varies from 0.5 to 1.5 cm long by 0.2 cm wide.

The thin film of the PEG* phase is modeled as a single layer with a different interfacial width (roughness) at the PEG*−air interface and the salt*−PEG* (liquid−liquid) interface. Adsorption of the ferritin protein at the liquid−liquid interface requires a more complicated model for the electron density profile. Inclusion of a second or third layer is adequate to describe these data. A general formula for the electron density gradient normal to a surface with *m* layers is[24]

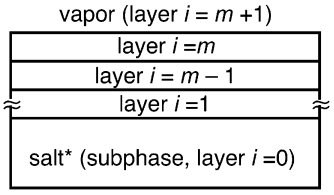


**Figure 2.** Nomenclature for layers. The PEG* film without ferritin has only one layer (subphase−layer−vapor). The fully developed ferritin film is described by three layers. Each interface has an interfacial width that characterizes the crossover of the composition of one layer (or bulk) to its neighboring layer.

$$\frac{d\langle\rho(z)\rangle}{dz} = \sum_{i=0}^{m}(\rho_i - \rho_{i+1})\frac{1}{(2\pi\sigma_{i+1}^2)^{1/2}}e^{-(z-D_i)^2/2\sigma_{i+1}^2} \quad (1)$$

where $\rho_0$ is the electron density of the subphase (salt* phase), $\rho_{m+1}$ is the density in air, $D_i = \sum_{j=1}^{i} L_j$ is the distance from the surface of the salt* phase to the interface between the *i*th and $(i + 1)$st layers, where $L_i$ is the thickness of the *i*th layer, and $\sigma_{i+1}$ is the interfacial width between the *i*th and $(i + 1)$st layers. The layer nomenclature is illustrated in Figure 2.

Given the electron densities of each layer and the subphase as well as the widths for each interface, the specular reflectivity is calculated from one of two standard methods. The first is the Born approximation for X-ray scattering, that relates the reflectivity to the electron density gradient normal to the interface, $d\langle\rho(z)\rangle/dz$ (averaged over the interfacial plane), and written as[25]

$$\frac{R(Q_z)}{R_F(Q_z)} \approx \left|\frac{1}{\rho_{\text{bulk}}}\int dz \frac{d\langle\rho(z)\rangle}{dz}\exp(iQ_z z)\right|^2 \quad (2)$$

where $\rho_{\text{bulk}}$ is the electron density of the bulk subphase and $R_F(Q_z)$ is the Fresnel reflectivity predicted for an ideal, smooth, and flat interface that has a step-function change in the electron density when going from one bulk phase to the other.[26] This Born approximation is only quantitatively accurate for regions of $Q_z > 3Q_c$ where $Q_c$ is the critical angle for total reflection. Because the reflectivity data for the ferritin include structure at low $Q_z$ we use the Parratt formalism to analyze that data.[27] In this formalism the exact reflection and transmission coefficients for each interface are used to calculate the specular reflectivity. As a guide to fitting the reflectivity data, the minimum number of layers is chosen that can reasonably account for the structure in the data. As described below, the fitting parameters usually correspond to qualitative features of the data.

### Thin Films without Ferritin

Figure 3 shows an example of $R/R_F$, the specular reflectivity normalized by the Fresnel reflectivity, as a function of the wave vector transfer normal to the interface $Q_z$ for a PEG3400 sample. The oscillations in the reflectivity are due to interference between X-rays reflected from the top and bottom of the layer. The decay of the oscillations in $R/R_F$ can be modeled by the presence of different interfacial widths at the liquid−vapor and liquid−liquid interfaces (for comparison, the dashed line in Figure 3 is the best fit with identical interfacial widths). The solid line is a fit to eqs 1 and 2 using a single-layer model ($m = 1$). This analysis yields the layer thickness $L_1 = 40.2 \pm 0.3$ Å, the liquid−liquid interfacial width $\sigma_1 = 7.9 \pm 0.3$ Å, the liquid−vapor width $\sigma_{\text{vapor}} = 2.9 \pm 0.2$ Å, and the electron

**TABLE 2: FittingParameters**[a]

| | layer 1 | | | layer 2 | | | layer 3 | | | |
|---|---|---|---|---|---|---|---|---|---|---|
| sample | $L_1$ (Å) | $\rho_1/\rho_{sub}$ | $\sigma_1$ (Å) | $L_2$ (Å) | $\rho_2/\rho_{sub}$ | $\sigma_2$ (Å) | $L_3$ (Å) | $\rho_3/\rho_{sub}$ | $\sigma_3$ (Å) | $\sigma_{vapor}$ |
| PEG3400 | $40.2^{\pm 0.3}$ | $0.86^{\pm 0.02}$ | $7.9^{\pm 0.3}$ | n/a | n/a | n/a | n/a | n/a | n/a | $2.9^{\pm 0.2}$ |
| calcd | n/a | $0.82^{\pm 0.02}$ | n/a | n/a | n/a | n/a | n/a | n/a | n/a | n/a |
| PEG8000 (w/o ferritin) | $52.0^{\pm 0.3}$ | $0.91^{\pm 0.02}$ | 18.2 | n/a | n/a | n/a | n/a | n/a | n/a | $3.1^{\pm 0.2}$ n/a |
| calcd | n/a | $0.90^{\pm 0.02}$ | n/a | n/a | n/a | n/a | n/a | n/a | n/a | n/a |
| PEG8000 (with ferritin) | | | | | | | | | | |
| 1.1 h | 42 | 1.06 | 19 | 44 | 0.92 | 21 | n/a | n/a | n/a | 2.4 |
| 18 h | 42 | 1.05 | 20 | 44 | 0.96 | 16 | n/a | n/a | n/a | 2.3 |
| 36 h[b] | $34^{+4/-14}$ | $1.03^{+0.04/-0.01}$ | $13^{+10/-5}$ | $54^{\pm 3}$ | $1.08^{\pm 0.006}$ | $10^{\pm 3}$ | $36^{\pm 1}$ | $0.955^{\pm 0.01}$ | $14^{\pm 1}$ | $2.8^{\pm 0.05}$ |
| salt* phase (with ferritin) | | | | | | | | | | |
| 12 h[c] | 14 | 1.1 | 5.0 | n/a | n/a | n/a | n/a | n/a | n/a | 3 |
| 28 h | $39^{\pm 2}$ | $0.965^{\pm 0.002}$ | $10.4^{\pm 2}$ | n/a | n/a | n/a | n/a | n/a | n/a | $2.9^{\pm 0.05}$ |

[a] Superscripts indicate error values on the fitting parameters, $L$ is the layer thickness, $\rho/\rho_{sub}$ is the layer electron density normalized by the electron density of the salt* subphase ($\rho_{sub} = 0.444$ e$^-$/Å$^3$ for PEG3400 and $\rho_{sub} = 0.374$ e$^-$/Å$^3$ for PEG8000), $\sigma_i$ is the interfacial width at the bottom of layer $i$, and $\sigma_{vapor}$ is the width at the interface with the vapor. [b] PEG8000 36 h data cannot be fit with a two-layer model and requires three layers. [c] There are large error values on this fit due to the limited range of $Q_z$, however $\rho_1/\rho_{sub} > 1.07$.

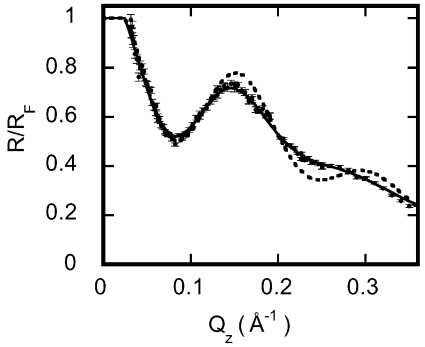


**Figure 3.** Specular reflectivity intensity normalized to the Fresnel reflectivity as a function of the wave vector transfer normal to the interface ($Q_z$) for a PEG3400 sample. The oscillations in the reflectivity are due to the interference between X-rays reflected from the top and bottom of the PEG* layer that is on top of the salt* subphase. The decay of the oscillations in $R/R_F$ can be modeled by the presence of different interfacial widths at the liquid−vapor and liquid−liquid interfaces (for comparison, the dashed line is the best fit with identical interfacial widths). Fits are further described in the text.

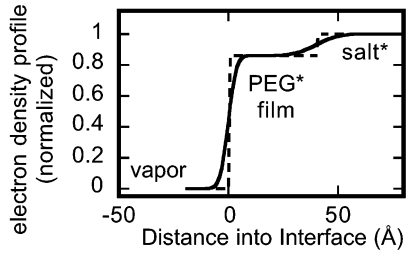


**Figure 4.** Real space profile of the thin PEG* film on top of the salt* phase. The electron density is normalized to the value of the bulk salt* phase. The dashed line represents a theoretical profile with interfaces of zero width (shown for comparison purposes only).

density of the film relative to the subphase, $\rho_1/\rho_{sub} = 0.86 \pm 0.02$ (see Table 2). The real space profile of electron density as a function of distance normal to the interface is shown in Figure 4.

The values of the fit parameters that determine this real space profile can be easily understood. The peak at $Q_z \approx 0.15$ Å$^{-1}$ corresponds to $2\pi/Q_{z,peak} \approx L_1$, the layer thickness. The width of the liquid−liquid interface is larger than the width of the liquid−vapor interface, $\sigma_1 \gg \sigma_{vapor}$, because the tension at the liquid−liquid interface is much smaller, $\gamma_1 \ll \gamma_{vapor}$ (where $\gamma_1 \equiv \gamma_{salt*/PEG*}$; see Table 1). According to capillary wave theory, we expect $\sigma \propto \gamma^{-1/2}$; therefore $\sigma_1/\sigma_{vapor} \approx (\gamma_{vapor}/\gamma_1)^{1/2}$, in agreement with our measurements ($\sigma_1/\sigma_{vapor} = 2.7 \pm 0.4$ and $(\gamma_{vapor}/\gamma_1)^{1/2} = 2.7 \pm 0.2$).[28] The electron density of the bulk PEG* phase divided by the bulk salt* phase is calculated to be $\rho_{bulk\ PEG*}/\rho_{sub} = 0.82 \pm 0.02$, close to our measurement of the electron density of the film normalized to the subphase.

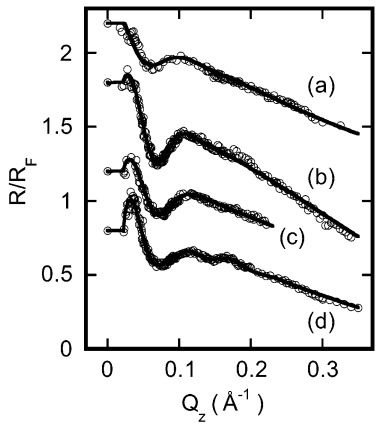


**Figure 5.** Reflectivity normalized to the Fresnel reflectivity as a function of wave vector transfer for the PEG8000 system (note that the units of $R/R_F$ are relative units; at low $Q_z$, $R/R_F = 1$; curves are offset for clarity): (a) without ferritin; (b) 1 h after adding ferritin; (c) 18 h after adding ferritin; (d) 36 h after adding ferritin. After 36 h a well-formed ferritin film is present.

The top curve of Figure 5a shows an example of $R/R_F$ for the PEG8000 sample. In comparison with Figure 3 it is seen that there are fewer oscillations. This is because the tension of the salt*−PEG* interface is much smaller for PEG8000 than for PEG3400. This results in a larger liquid−liquid interfacial width (roughness) for the PEG8000 system ($\sigma_1 = 18.2$ Å). The intensity of X-rays reflected from a rougher interface are more quickly reduced as a function of $Q_z$, because $R/R_F \propto \exp(-\sigma^2 Q_z^2)$, thereby significantly reducing the amplitude of the interference fringes at higher $Q_z$.

The measured electron density of the PEG8000 film is the same as that calculated for the bulk PEG* phase (for the PEG8000 system, see Table 2). The layer thickness $L_1 = 52.0 \pm 0.2$ Å is larger than that for the PEG3400 system. Although it may be tempting to try to relate the ratio of the layer thickness for these two systems to some ratio of their gyration radii, we

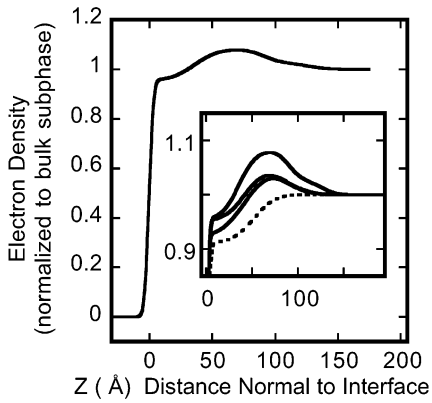


**Figure 6.** Real space profile of the electron density (averaged over the plane of the interface) as a function of the distance normal to the interface. The vapor is at negative *z*. The main figure illustrates the ferritin layer equilibrated for 36 h. The inset illustrates the interfacial region without ferritin (dotted line) and for progressive times after adding ferritin (1, 18, and 36 h, from bottom to top). After 36 h a well-formed ferritin film is present.

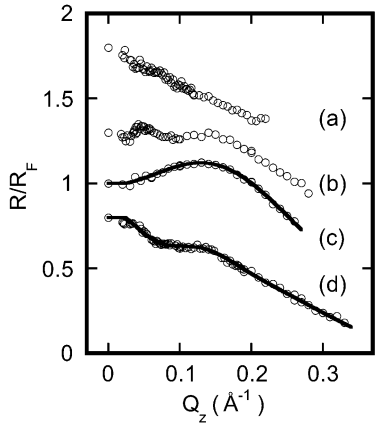


**Figure 7.** Control experiment for the addition of ferritin without the presence of the PEG* film: (a) without ferritin; (b)−(d) 1, 12, and 28 h after adding ferritin. Although some ferritin initially goes to the interface (as indicated by the first peak in (b)), the final state of the film does not contain a ferritin layer (indicated by the absence of a low $Q_z$ peak in (d)).

do not believe this is valid because the thickness depends on the precise location in the phase diagram of this three-component system. For example, we have measured films of PEG3400 with a thickness greater than 52 Å for different concentrations of the components of the PEG3400 system.

Our measurements indicate that the layer is a thin film of a PEG* solution rather than a monolayer of PEG molecules adsorbed to the interface. The electron density of the film for each sample is similar to the electron density of the bulk PEG* phase (Table 2). The difference in electron density between the two films is accounted for by the difference in PEG monomer concentrations in the bulk solutions. Also, a monolayer of PEG has a measured thickness of 10 Å, less than the thickness of our film.[29] Finally, the radius of gyration of our PEG under similar conditions has been measured to be close to 10 Å, also less than the film thickness.[30]

### Thin Films with Ferritin

Figure 5 illustrates the time sequence of X-ray reflectivity measurements after adding ferritin protein to the subphase. Curve a is the PEG8000 system before the protein was added and is shown for comparison. The reflectivity measurements shown were started approximately 1, 18, and 36 h after the ferritin was added. Each measurement takes approximately 4 h. Within an hour or so after adding the ferritin, it is clear that the reflectivity curve has been affected. By 18 h, a peak at low $Q_z$ (=0.034 Å$^{-1}$) is clearly apparent and increases in intensity with time. This peak's maximum is greater than 1, a clear indication that a higher electron density species is adsorbing to the interface. At the longest time measured (36+ hours) a higher $Q_z$ peak (at $Q_z \approx 0.17$ Å$^{-1}$) also appears.

As previously discussed, the PEG8000 system without ferritin can be fit with a single-layer model of the electron density profile. The peak that appears at $Q_z = 0.034$ Å$^{-1}$ requires the addition of a second layer to the model, and the three peaks appearing in the 36 h curve require a total of three layers (i.e., the 36 h data cannot be fit with a two-layer model). The parameters for these fits are given in Table 2. The real space models of the electron densities are shown in Figure 6. These models indicate that the ferritin quickly adsorbs to the interface, but initially there is so much disorder that the X-rays primarily detect just an increase in electron density at the interface. However, at the longest time measured the amount of ferritin adsorbed has increased significantly and has formed a two-dimensional film that is ordered normal to the interface. In addition to the increase in the peak amplitude, there is a shoulder in the electron density on the side of the peak adjacent to the salt* phase.

Note that monolayer adsorption of the ferritin was successful with the PEG8000 system, but not with the PEG3400 system. In the PEG3400 system the ferritin precipitated at the interface to form large patches that did not spread further. We suspect that this difference is due to the much larger salt content in the salt* phase of the PEG3400 system, though it is also possible that the thinner PEG3400 films do not allow the ferritin proteins to fully spread across the interface.

**Control Experiment, Addition of Ferritin to the Salt-Rich Phase without the PEG* Film.** As a control experiment, we added ferritin to the salt-rich subphase when the thin film of PEG* phase was not present (i.e., a drop of the PEG* phase had not been previously added to the surface of the salt* phase). Figure 7 illustrates the time sequence of X-ray reflectivity measurements after adding ferritin protein to the subphase. The parameters for the fits are given in Table 2. Before adding the ferritin, the single interface of the salt* phase with vapor yields a featureless X-ray reflectivity curve, as expected for a simple liquid interface without an adsorbed layer (see Figure 7a). About an hour after adding the ferritin, the presence of a small peak at low $Q_z \approx 0.04$ Å$^{-1}$ provides some evidence of a higher electron density at the interface due to ferritin adsorption; see Figure 7b. An additional broader peak at $Q_z \approx 0.15$Å$^{-1}$ may indicate the formation of a thin layer. However, by 12 h, the small peak at low $Q_z \approx 0.04$Å$^{-1}$ has disappeared, leaving only a broad peak indicative of a single very thin layer, but with a higher electron density than the salt-rich phase; see Figure 7c. This may be denatured ferritin. By 28 h, a thin layer has formed that is similar to the thin PEG* layers that are formed by addition of a drop (compare to Figure 5a), but with a higher electron density than expected for a PEG* phase although it is less than the salt-rich subphase; see Figure 7d.

Because the ferritin was added to the salt-rich subphase in drops of the PEG* phase, it is likely that the lighter PEG* phase has risen to the surface of the salt-rich phase and formed a thin layer in combination with some denatured ferritin. It is not clear what happened to the ferritin, but we suspect that the ferritin initially goes to the surface of the salt-rich phase and is irreversibly denatured at this interface with the vapor. This

control experiment shows that the thin film of PEG* phase must be present before the addition of ferritin to stabilize the ferritin in its natural form at the aqueous-aqueous interface.

## Discussion

**PEG* Films without Ferritin.** Our results show that the addition of a drop of PEG* phase on top of the salt* bulk phase produces a film of PEG* phase that is several nanometers thick in equilibrium with macroscopic lenses (droplets) of the PEG* phase. The spreading coefficient $S = \gamma_{\text{salt*/air}} - (\gamma_{\text{salt*/PEG*}} + \gamma_{\text{PEG*/air}})$ can be computed from our tension measurements (see Table 1) and is positive for both of the systems studied ($S_{\text{PEG3400}} = 18.6$ mN/m and $S_{\text{PEG8000}} = 2.4$ mN/m). Note that the measurement of $\gamma_{\text{salt*/air}}$ is on an interface without the PEG* layer and is, therefore, the correct tension to use to calculate $S$.

A positive initial spreading coefficient is often taken to indicate complete wetting. Although the PEG* drops initially spread completely across the interface, the final configuration consists of a very thin film in coexistence with macroscopic lenses (flattened drops). Brochard-Wyart et al. discussed this possibility by analyzing the free energy $F$ (per unit area) of a spreading film of thickness $l$, written as[31]

$$F(l) = \gamma_{\text{salt*/PEG*}} + \gamma_{\text{PEG*/air}} + \Delta G(l) \tag{3}$$

where $\Delta G(l)$ is an excess free energy that depends on the layer thickness. For large $l$, $\Delta G(l)$ tends to zero. As one example, $\Delta G(l)$ can be written to include a repulsive short-range force and an attractive long-range van der Waals interaction, written as[32]

$$\Delta G(l) = S_{\text{p}} \exp[(l_{\text{o}} - l)/\Lambda] - \frac{A_{\text{eff}}}{12\pi l^2} \tag{4}$$

where $S_p$ is the amplitude of the short-range interaction, $A_{\text{eff}}$ is an effective Hamaker constant, and $l_{\text{o}}$ sets the distance for the hard core repulsion. The first term in eq 4 models a short-range repulsive interaction with decay length $\Lambda$. It has been predicted that mutual hindrance of capillary waves leads to an effective entropic repulsion between the interfaces, which is exponential,[33,34] though other short-range interactions may also contribute to this decay length. The second term is the van der Waals interaction between two planar interfaces separated by a distance $l$. For $A_{\text{eff}} > 0$, Brochard-Wyart et al. predicted pseudopartial wetting in which a thin film exists in coexistence with macroscopic lenses, similar to our observations.[31] The excess free energy in eq 4 has also been used to discuss instabilities in thin films similar to the breakup we observed in the spreading kinetics (see Figure 2).[32] We plan more detailed measurements of this instability to further explore the relationship with theory.

We have shown elsewhere that the excess free energy $\Delta G(l)$ leads to a coupling between the capillary wave fluctuations on the two nearby interfaces (the salt*−PEG* liquid−liquid interface and the PEG*−air liquid−vapor interface).[18] This coupling can be measured with X-ray off-specular diffuse scattering that is sensitive to the height fluctuations due to capillary waves on both interfaces. A measurement of the PEG3400 system allowed us to determine three of the parameters in eq 4 when the fourth parameter, $l_{\text{o}}$, was assumed to be in the range from 1 Å $< l_{\text{o}} <$ 3 Å. This analysis yielded $\Lambda \approx 2.9$ Å, $S_{\text{p}} \approx 18.7$ mN/m, and the Hamakar constant $A_{\text{eff}} \approx 8 \times 10^{-23}$ J. Seifert calculated the decay length, $\Lambda$, for a single membrane (with finite tension) interacting with a hard wall.[34] Diamant recently extended this calculation to two interacting membranes (with tension), as in our system.[35] Diamant's calculation leads to $\Lambda = [k_{\text{B}}T(\rho_{m,1} + \rho_{m,2})^2/4\pi(\gamma_1\rho_{m,2}^2 + \gamma_2\rho_{m,1}^2)]^{1/2} = 2.3$ Å, close to our measured value (where $\rho_{m,1}$ is the mass density difference between the PEG* and salt* phases, $\rho_{m,2}$ is the mass density difference between the PEG* and vapor phase, with $\rho_{m,\text{PEG*}} = 1.11$ g/cm$^3$ and $\rho_{m,\text{salt*}} = 1.38$ g/cm$^3$, and $\gamma_1 \equiv \gamma_{\text{salt*/PEG*}}$, $\gamma_2 \equiv \gamma_{\text{PEG*}}$; see Table 1). As discussed by Brochard-Wyart et al., the sign of the Hamakar constant and the spreading coefficient are consistent with our observation of macroscopic drops in equilibrium with a very thin layer that covers the interface, though we have chosen a different sign convention for the effective Hamakar constant.[31] The effective Hamakar constant is the difference between two Hamakar constants, $A_{\text{eff}} = A_{\text{PEG*,PEG*}} - A_{\text{PEG*,salt*}}$. $A_{\text{eff}}$ is small ($\sim k_{\text{B}}T/50$), indicating that the attraction of the upper phase for the lower phase is only slightly different from the attraction of the upper phase to itself.

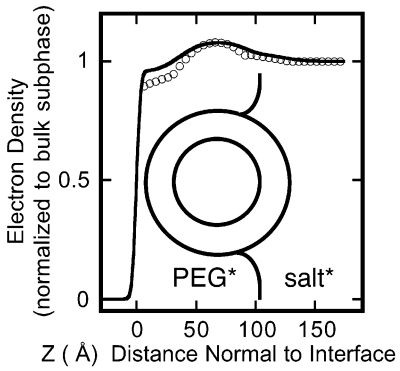


**Figure 8.** Electron density profile of ferritin adsorbed at the PEG*/salt* interface. Solid curve is the fit profile (same as Figure 6), dots are a calculation of the profile assuming an arrangement of the ferritin proteins at the interface as described in the text. The cartoon represents (to scale) the position of the ferritin used for the calculation. The regions bounded by the two concentric circles represent the core and shell of the ferritin. The curved meniscus demarcating the boundary of the salt* and PEG* phases schematically indicates that the measured density of the aqueous solvent in that region is between the salt* and PEG* densities.

**PEG* Films with Ferritin.** A ferritin molecule is nearly spherical with a radius of 61 Å and consists of a shell surrounding a core with a radius of 37 Å composed primarily of hydrated iron oxide.[36] The ferritin we used has approximately 17.6 wt % of iron, so only 69% of the ferritin molecules contain the iron core (assuming that the core is either full or empty). Figure 8 illustrates a simple model for the ferritin that locates the protein at the salt*−PEG* interface with the lower part of its shell in the salt* phase and the rest of the ferritin in the PEG* phase. The perimeter of the ferritin is displaced from the vapor interface by 6 Å. The salt*−PEG* interface is near the level of the bottom of the ferritin core. The average density in the aqueous solution at this level is between that of the salt* and PEG* phases. This may indicate a preferential attraction of the salt* phase for the ferritin (indicated schematically by the meniscus in Figure 8). The resultant electron density for this model is shown, ignoring the effect of interfacial roughness (zero interfacial width).[37] This model is in reasonable agreement with the measured electron density profile, also shown in Figure 8. The area per ferritin molecule is determined to be 350 nm$^2$ by matching the peak electron density from the measured profile. This is larger than the close packed value of 146 nm$^2$/molecule and indicates that the ferritin molecules are either very loosely packed or the interface consists of regions of close packed ferritin and areas without ferritin.[8] Our reflectivity measurements

cannot distinguish between these two possibilities. Also, grazing incidence diffraction measurements from the surface did not contain any diffraction peaks, indicating that crystalline ordering of the ferritin was not present in our system. The primary discrepancy between the calculated and measured values of the electron density profile occurs near the vapor interface where the measured electron density is slightly higher than predicted from our simple model.

After inserting drops of ferritin in PEG* phase into the lower salt* phase, the drops rise to the surface because the ferritin-PEG* solution is lighter than the salt* phase. Our measurements indicate that the ferritin is mostly surrounded by PEG* phase in the final configuration, though the ferritin is straddling the salt*−PEG* interface. This may be a result of the preferred contact angle at the contact line between the salt* and PEG* phases and the outer shell of the ferritin. However, it may also be the result of a salting-out of the ferritin from the high salt concentration salt* phase and further confinement by the available PEG* thin film.

This technique is currently limited to studying proteins that are resistant to the relatively high salt concentration of the PEG8000 system (∼1 M). Currently, we have only tried this technique with one protein (ferritin), though we anticipate that it will be useful to study adsorption of other proteins. In addition, there are many possibilities for forming biphase aqueous systems, including polymer−polymer systems that do not require any salt for phase separation.[1,2] These may allow this technique to be used to study a wider range of proteins or other two-dimensional biomolecular structures at the aqueous-aqueous interface.

In summary, we used X-ray reflectivity to demonstrate that aqueous films of several nanometers thickness can be formed on top of aqueous bulk phases using biphase systems consisting of PEG, potassium phosphates, and water. These films are not monolayers, but rather are equilibrium thin films of the PEG-rich phase of the biphasic system. Our observations are consistent with a thin film free energy proposed by Brochard-Wyart et al. to describe pseudopartial wetting in which a thin film coexists with macroscopic drops at an interface.[31] We have also demonstrated that ferritin proteins injected into the bulk aqueous phase can adsorb to the thin film to form a monolayer of proteins that is ordered in the direction normal to the interface. We anticipate that future experimentation with other proteins and, possibly, other biphasic systems will provide interesting opportunities to study protein ordering.

**Acknowledgment.** We acknowledge the assistance of Aleksey M. Tikhonov (University of Chicago and Brookhaven National Laboratory) in the X-ray measurements. This research was partially supported by the Chemical Technology Division at Argonne National Laboratory and NSF Division of Materials Research. Brookhaven National Laboratory is supported by DOE.

## References and Notes

(1) Albertsson, P. A. *Partition of Cell Particles and Macromolecules*; Wiley: New York, 1986.

(2) Zaslavsky, B. Y. *Aqueous Two-Phase Partitioning Physical Chemistry and Bioanalytical Applications*; Marcel Dekker: New York, 1995.

(3) Harris, J. M. *Poly(ethylene glycol) Chemistry: Biotechnical and Biomedical Applications*; Plenum Press: New York, 1992.

(4) Elbert, D. L.; Hubbel, J. A. *Annu. Rev. Mater. Sci.* **1996**, *26*, 365.

(5) Abuchovski, A.; Davis, F. F. In *Enzymes as Drugs*; Holsenberg, J., Roberts, J., Eds.; Wiley: New York, 1981.

(6) Efremova, N. V.; Sheth, S. R.; Leckband, D. E. *Langmuir* **2001**, *17*, 7628.

(7) Michel, H. *Crystallization of Membrane Proteins*; CRC Press: Boca Raton, FL, 1991.

(8) Nagayama, K.; Takeda, S.; Endo, S.; Yoshimura, H. *Jpn. J. Appl. Phys.* **1995**, *34*, 3947.

(9) Dimitrov, A. S.; Yamaki, M.; Nagayama, K. *Langmuir* **1995**, *11*, 2682.

(10) Yoshimura, H.; Scheybani, T.; Baumeister, W.; Nagayama, K. *Langmuir* **1994**, *10*, 3290.

(11) Aoyama, K.; Ogawa, K.; Kimura, Y.; Fujiyoshi, Y. *Ultramicroscopy* **1995**, *57*, 345.

(12) Darst, S. A.; Edwards, A. M. *Curr. Opin. Struct. Biol.* **1995**, *5*, 640.

(13) Kornberg, R. D.; Ribi, H. O. *Protein Structure, Folding, and Design 2*; Oxender, D. L., Ed.; Alan R. Liss, Inc.: New York, 1987; p 175.

(14) Brown, P. O.; Kubalek, E. W.; Grice, S. F. L. *J. Struct. Biol.* **1994**, *113*, 117.

(15) Frey, W.; Schief, W. R.; Pack, D. W.; Chen, C. T.; Chilkoti, A.; Stayton, P.; Vogel, V.; Arnold, F. H. *Proc. Natl. Acad. Sci. U.S.A.* **1996**, *93*, 4937.

(16) Hebert, H. *Biomed. Health Res.* **1998**, *20*, 88.

(17) Hasler, L.; Heymann, J. B.; Engel, A.; Kistler, J.; Walz, T. *J. Struct. Biol.* **1998**, *121*, 162.

(18) Li, M.; Tikhonov, A. M.; Chaiko, D.; Schlossman, M. L. *Phys. Rev. Lett.* **2001**, *86*, 5934.

(19) Schlossman, M. L.; Li, M.; Mitrinovic, D. M.; Tikhonov, A. M. *High Perf. Polym.* **2000**, *12*, 551.

(20) Lando, J. L.; Oakley, H. T. *J. Colloid Interface Sci.* **1967**, *25*, 526.

(21) Adamson, A. W. *Physical Chemistry of Surfaces*, 5th ed.; John Wiley & Sons: New York, 1990.

(22) Schlossman, M. L.; Synal, D.; Guan, Y.; Meron, M.; Shea-McCarthy, G.; Huang, Z.; Acero, A.; Williams, S. M.; Rice, S. A.; Viccaro, P. J. *Rev. Sci. Instrum.* **1997**, *68*, 4372.

(23) Schlossman, M. L.; Pershan, P. S. In *Light Scattering by Liquid Surfaces and Complementary Techniques*; Langevin, D., Ed.; Marcel Dekker Inc.: New York, 1992; pp 365−403.

(24) Tidswell, I. M.; Ocko, B. M.; Pershan, P. S.; Wasserman, S. R.; Whitesides, G. M.; Axe, J. D. *Phys. Rev. B* **1990**, *41*, 1111.

(25) Pershan, P. S. *Faraday Discuss. Chem. Soc.* **1990**, *89*, 231.

(26) Born, M.; Wolf, E. *Principles of Optics*, 6th ed.; Pergamon Press: Oxford, England, 1980.

(27) Parratt, L. G. *Phys. Rev.* **1954**, *95*, 359.

(28) Buff, F. P.; Lovett, R. A.; Stillinger, F. H. *Phys. Rev. Lett.* **1965**, *15*, 621.

(29) Benderson, J. A.; Richards, R. W.; Penfold, J.; Thomas, R. K.; Lu, J. R. *Macromolecules* **1993**, *26*, 4591.

(30) Thiyagarajan, P.; Chaiko, D. J.; Hjelm, R. P. *Macromolecules* **1995**, *28*, 7730.

(31) Brochard-Wyart, F.; Meglio, J.-M. d.; Quere, D.; Gennes, P. G. d. *Langmuir* **1991**, *7*, 335.

(32) Sharma, A.; Khanna, R. *Phys. Rev. Lett.* **1998**, *81*, 3463.

(33) Dietrich, S.; Nightingale, M. P.; Schick, M. *Phys. Rev. B* **1985**, *32*, 3182.

(34) Seifert, U. *Phys. Rev. Lett.* **1995**, *74*, 5060.

(35) Haim Diamant, personal communication.

(36) Fischbach, F. A.; Anderegg, J. W. *J. Mol. Biol.* **1965**, *14*, 458.

(37) The electron densities used for this calculation are as follows: 0.335 $e^-/Å^3$ for PEG*; 0.374 $e^-/Å^3$ for salt*; 0.769 $e^-/Å^3$ for the average ferritin core; 0.41 $e^-/Å^3$ for the ferritin shell.